On the Identification of High Energy Cosmic Ray Electrons in the Advanced Thin Ionization Calorimeter (ATIC)

W.K.H. Schmidt[1]**, Jin Chang**[1,3]**, Opher Ganel**[2]**, Eun-Suk Seo**[2]**, Ramin Sina**[2]**, Jian-Zhong Wang**[2]
For the ATIC Collaboration
[1] *Max-Planck-Institut für Aeronomie, D-37191 Katlenburg-Lindau, Germany*
[2]*Institute for Physical Science and Technology, University of Maryland, College Park, MD20742*
[3] *Purple Mountain Observatory* Academia Sinica, Nanjing, China

Abstract

ATIC is specifically designed for high energy cosmic ray ion detection. We have investigated the possibility to identify high energy primary cosmic ray electrons in the presence of the 'background' of cosmic ray protons by simulating nuclear-electromagnetic cascade showers in the dense material of the calorimeter using the GEANT computer code. We find that the design consisting of a graphite target and an energy detection device, a totally active calorimeter built up of 2.5 cm x 2.5 cm x 25.0 cm BGO scintillator bars, gives us sufficient information to distinguish electrons from protons reasonably well. While identifying about 70% of electrons as such, only about one in 10,000 protons will mimic an electron. If confirmed later this year by calibration at CERN, this will make ATIC a fine high energy electron sensing instrument.

1   Introduction

ATIC is an ionization calorimeter for the measurement of very high energy cosmic rays at balloon altitudes during long duration balloon flights. A full description of the instrument is given elsewhere in these proceedings (Guzik, et al., 1999; Ganel, et al., 1999). This instrument is dedicated to the observation of protons and heavy nuclei up to the highest possible energies ($\approx 10^{14}$ eV). It consists of a target of 3/4 proton interaction lengths (30 cm) of graphite followed by about 22 radiation lengths (25 cm, equivalent to about 1.1 proton interaction lengths) of Bismuth Germanate (BGO) scintillator. The graphite target (comprising only 1.6 radiation lengths) is there to force as many protons as possible to interact early in the instrument, so that the conditions for the ensuing shower development are similar for all events.

The shower detector is a totally active calorimeter that consists of 10 layers of BGO bars of 2.5 cm by 2.5 cm cross sectional area and 25 cm length. Sets of 40 such bars are arranged in 50 cm x 50 cm layers. Each layer has its bars at right angle with respect to its neighbor(s). This way the shower is observed in three dimensions so that its axis can be reconstructed. The 2.5 cm segmentation in the BGO and 2 cm segmentation in three plastic scintillator layer pairs interleaved with the graphite layers should provide sufficient resolution for the determination of the impact point of the primary showering particle to better than a centimeter or so (Ganel, & Seo, 1998). For the observation of protons and light nuclei this information is used to identify the incoming primary among the abundant backscattered/backemitted particles from the shower.

In dedicated cosmic ray experiments - past, present, and future - special features are often included to help separate electrons from protons while not compromising too much the primary goal of measuring the properties of hadrons and heavier nuclei. We have taken a different approach by taking the cosmic-ray instrument (in this case ATIC) and try to achieve the best possible separation within the constraints of the given design.

An uncertainty here is the atmospheric background. Estimates (cf Nishimura, et al., 1980) and our own simulations indicate an atmospheric electron flux of around 10% of the cosmic flux level at 1 TeV at 4 mb residual atmosphere (being very sensitive to the atmospheric pressure). As the residual air mass above the balloon will likely fluctuate during the flight by 20% or so, we will estimate the relative contributions of the variable atmospheric and the constant cosmic flux components wherever the statistical sample is sufficient. Thus a minimum result will be an empirical estimate of the atmospheric background.

The fact that most of the protons interact in the target makes the beginning point distributions of showers, that have been used in the past for distinguishing primary electrons from primary protons (cf Silverberg,

et.al., 1973, Atallah, et al., 1975), practically useless for this purpose in this design. Therefore we are using other means, exploiting the (albeit limited) lateral resolution of the shower energy deposition provided by the segmentation of the plastic scintillators and calorimeter.

2 Electron-Proton Distinction

Electron identification in ATIC is achieved by using the following procedure.

(a) By simulation we have obtained average shower curves for primary electrons. We find that there are differences between the shower curves determined analytically using Rossi's and Greisen's Approximation A (Rossi, 1952) that have been used in the past (cf Silverberg, et al., 1973) and the simulations using the GEANT computer code (Brun et al., 1984). In addition Monte Carlo simulations can cope easily with the presence of different materials in the shower detector, which is much more difficult to include in analytical calculations (cf Pinkau, 1965; Crannell, et al.,1969).

We find that primary electrons deposit about 97% of their energy in the BGO calorimeter while protons deposit about 40%. In this paper we always compare proton and electron events with the same total energy
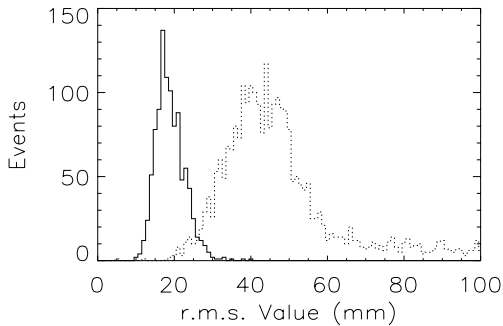

Figure 1: Comparison of the widths of showers initiated by electrons (solid line) and protons (dashed line) as determined by the r.m.s.-value of signals about the shower axis in the BGO scintillator bars in the top BGO layer, BGO1.

deposit in the calorimeter.

For simulated events we first compute the trajectory of the incoming particle from the three dimensional shower information inside the calorimeter. Then we try to fit the longitudinal shower curve of an event with a particular energy deposit to the average shower curve corresponding to an electron event of the same energy deposit. By requiring a goodness of fit as expressed by χ^2 per degree of freedom of less than 0.5 we lose 5% of the electrons but reject 68% of the protons in this first step.

(b) In the next step we make use of the lateral distribution of energy deposit. Particularly the top calorimeter layer BGO1 shows good discrimination between electrons and protons as shown in Figure 1. Here the projected width of the shower around its momentum trajectory is expressed by its r.m.s. value. The r.m.s.-value distributions of electron and proton events of the same energy deposit are well separated. Deeper in the calorimeter this separation is lost

(c) Next we consider the backscattered/backemitted energy flux, which is different for the two species of primary particles. The number of backscattered particles from proton events is substantially higher than that from electron events, and owing to the segmentation of the plastic scintillators interleaved with the target a measure for this number can be determined for each
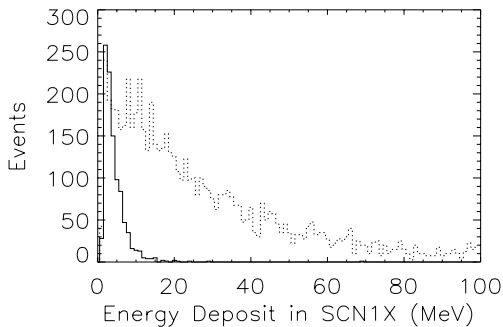

Figure 2: Comparison of the energy deposition of electrons (solid line) and protons (dashed line) in the topmost (plastic) scintillator SCN1X (X-coordinate).

event. In addition, there is a difference in types and fluxes of the backscattered particles. In proton events a large part of the upwards flux consists of ionizing particles, while in electron events it consists mostly of low energy photons which deposit often much less per event than the >2 MeV of a penetrating charged particle.

Figure 2 shows the difference in energy deposition distributions in the topmost plastic scintillator SCN1X

of events with calorimeter energy deposit of about 1 TeV. The distributions of the number of strips with energy deposit of >1 MeV due to backscattered events, a measure for the total number of backscattered particles, look rather similar to Figure 2 for the same SCN1X.
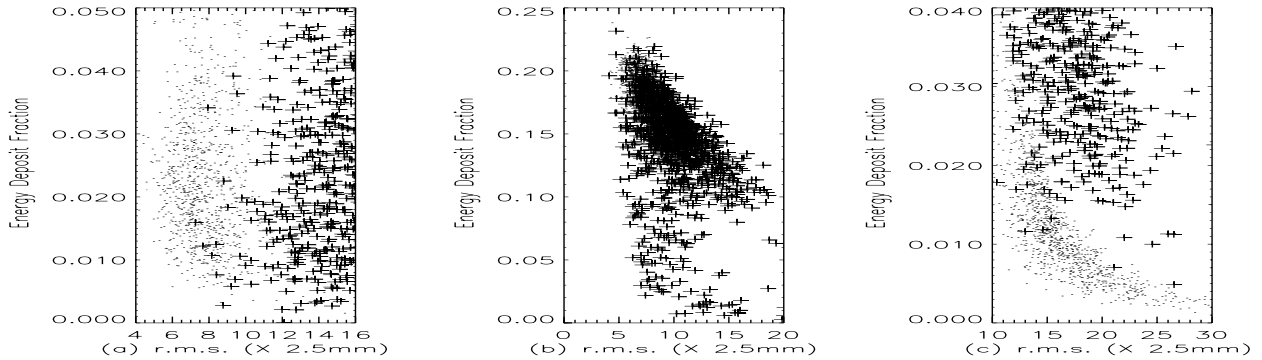

Figure 3: Scatter plots of energy deposits of individual events vs. width of showers (expressed as r.m.s. values) at three different depths in the BGO calorimeter (+ proton events, . electron events): (a) BGO1; (b) BGO5; (c) BGO10. For explanation see text.

(d) Although deep in the calorimeter the width distributions for electron and proton primaries overlap more and more we have found one more place with useful information. Consider Figure 3a to 3c: Here we show scatter plots of the shower energy deposit in individual BGO layers, expressed as a fraction (En) of the total energy deposit (Sum) in the calorimeter, on the ordinate, vs. shower width expressed as the r.m.s. value on the abscissa. The best electron-proton distinction criterion in BGO1 is the shower width alone (see also Figure 1). In BGO5 the two populations overlap substantially, but towards the bottom of the calorimeter the populations separate again, however not in either shower width or energy deposit alone.

Here we define a function $F = (En/Sum) * r.m.s.^2$. If we plot the F-value distributions for BGO10 we obtain Figure 4. The separation of the two distributions is about as good as in Figure 1. This again helps to suppress the proton 'background' from the point of view of electron observations. Incidentally, if the scatter plot of Figure 3c were taken by itself, about 99% of the proton events would be rejected in this step alone

3   Result

Taken all together we find that by using the above criteria we identify about 70% of the electrons as such, but only two and one in 10,000 protons mimic electrons at around 500 GeV and 1 TeV, respectively. The proton rejection power increases slightly with increasing energy, a trend in the right direction as the proton/electron flux ratio increases as well. If this result is confirmed by calibration measurements at CERN later this year, we find that while the electron-proton distinction with ATIC may not be as strong as claimed for other calorimeter configurations (10^{-5} is often claimed/required, cf Ormes, et al., 1997), it is sufficient to facilitate cosmic ray electron observation to the highest energies commensurate with long duration balloon flights. Note that we always refer to protons and electrons with the same total energy deposit in the calorimeter, not incident energy of protons nor total cosmic ray flux of protons.
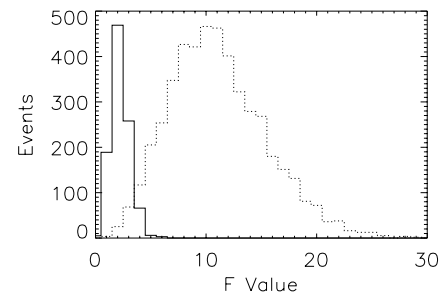

Figure 4:   F-value distributions (see text) for electrons (solid line) and protons (dashed line) for the signals in the last calorimeter layer BGO10.

In order to convince ourselves of the latter point we have assumed the following spectra of the various cosmic ray components: CR protons: $J_p = 1.94 * 10^4 * E^{-2.75}$/(m^2*s*sr*GeV) (Webber,1997); CR electrons: $J_e = 5.72 * 10^2 * E^{-3.26}$/(m^2*s*sr*GeV) (Wiebel-Sooth et al.,1995); CR gamma-rays (diffuse): $J_\gamma = 1.28 * 10^{-2} * E^{-2.12}$/(m^2*s*sr*GeV) (Fichtel, & Trombka, 1997); Atmospheric gamma-rays at 4 mb balloon altitude: $J_{a\gamma} = 37.9 * E^{-2.75}$/(m^2*s*sr*GeV) (Nishimura, et al., 1980).

Taking these numbers at face value we find that in a balloon flight of 10 days we expect to detect about 19 cosmic ray electrons between 500 GeV and 1 TeV, and 1 proton mimicking an electron in the same total energy deposit interval in the calorimeter. In an accompanying paper at this conference (Chang, et al., 1999) we have studied the possibility of using ATIC for cosmic gamma-ray observations as well. One side result of that study is that a fraction of gamma-ray events will mimic electrons. In the high gamma-ray background of atmospheric origin that means that in addition to 19 cosmic electrons about 2 gamma-ray events would mimic electrons (at 4 mb balloon float level). So it is the atmospheric gamma-ray background that affects the observation of cosmic electrons more than the protons.

4 Summary and Conclusions

In this paper we have described the results of simulation calculations carried out in order to find a way to identify electrons among the abundant cosmic ray protons in the expected balloon flight data of the ionization calorimeter ATIC. Our approach is to take the calorimeter as it is, optimized for the detection of cosmic ray protons and heavier nuclei. We have not attempted to suggest design compromises or optimization for easier distinction between electrons and protons. We have shown that using extrapolations of presently available data, we would expect at 1 TeV about one background event from protons per twenty electron events. A somewhat higher background must be expected from atmospheric gamma-rays at a typical balloon altitude for charged cosmic ray particle observation.

The main reasons for reasonable success in identifying electrons are that both the ionization calorimeter and the plastic scintillators used for triggering and charge identification allow some lateral spatial resolution. It also helps that the shower detector is totally active.

We want to emphasize that we are not suggesting that the ATIC configuration is ideal for electron observations. Rather, we are trying to point out that the electron-proton discrimination power of ATIC is sufficient to warrant meaningful cosmic ray electron observations at high energy.

References

Atallah, et al., 1975, Nucl. Instr. Meth. 124, 461-476

Brun,R., et al., CERN DD/EE/84-1 (Geneva) 1984

Crannell, C.J., et al., 1969, Phys.Rev. 182, 1435-1440

Fichtel, C.E., & Trombka, J.I. 1997, Gamma-Ray Astrophysics (NASA Ref.Pub. 1386), p.221

Ganel, O., & Seo, E.S., 1998, Cospar 32, Nogoya, Japan

Ganel, O., et al., Proc. 26th ICRC (Salt Lake City 1999), paper code OG 4.6.01

Guzik, T.G., et al., Proc. 26th ICRC (Salt Lake City 1999), paper code OG 4.1.03

Nishimura, J., et al. 1980, ApJ 238, 394-409

Ormes, J., et al., 1997, Proc. 25th ICRC (Durban 1997), 5, 73

Pinkau, K., 1965, Phys. Rev. 139, B1548-B1555

Rossi, B., 1952, High Energy Particles (Prentice Hall, New York), p.251

Silverberg, R.F., Ormes, J.F., & Balasubrahmanyan, V.K., 1973, J.Geophys.Res. 78, 7165-7173

Webber, W.R. 1997, Space Sci.Rev. 81, 107-142

Wiebel-Sooth, Barbara, et al., Proc. 24th ICRC (Rome 1995), 3, 45